International Journal of Minerals, Metallurgy and Materials
Volume 22, Number 7, July 2015, Page 704
DOI: 10.1007/s12613-015-1125-8

Effect of arsenic content and quenching temperature on solidification microstructure and arsenic distribution in iron–arsenic alloys

Wen-bin Xin[1,2], *Bo Song*[1,2], *Chuan-gen Huang*[1,2], *Ming-ming Song*[1,2], *and Gao-yang Song*[1,2]

1) State Key Laboratory of Advanced Metallurgy, University of Science and Technology Beijing, Beijing 100083, China
2) School of Metallurgical and Ecological Engineering, University of Science and Technology Beijing, Beijing 100083, China
(Received: 8 August 2014; revised: 20 October 2014; accepted: 22 October 2014)

Abstract: The solidification microstructure, grain boundary segregation of soluble arsenic, and characteristics of arsenic-rich phases were systematically investigated in Fe–As alloys with different arsenic contents and quenching temperatures. The results show that the solidification microstructures of Fe–0.5wt%As alloys consist of irregular ferrite, while the solidification microstructures of Fe–4wt%As and Fe–10wt%As alloys present the typical dendritic morphology, which becomes finer with increasing arsenic content and quenching temperature. In Fe–0.5wt%As alloys quenched from 1600 and 1200°C, the grain boundary segregation of arsenic is detected by transmission electron microscopy. In Fe–4wt%As and Fe–10wt%As alloys quenched from 1600 and 1420°C, a fully divorced eutectic morphology is observed, and the eutectic Fe_2As phase distributes discontinuously in the interdendritic regions. In contrast, the eutectic morphology of Fe–10wt%As alloy quenched from 1200°C is fibrous and forms a continuous network structure. Furthermore, the area fraction of the eutectic Fe_2As phase in Fe–4wt%As and Fe–10wt%As alloys increases with increasing arsenic content and decreasing quenching temperature.

Keywords: iron–arsenic alloys; solidification; microstructure; segregation; eutectic

1. Introduction

Arsenic is one of the common residual elements in steel and mainly comes from iron ore, scrap steel, ferroalloy, and other furnace charge [1]. With the recycling of scrap steel and the utilization of iron ore containing arsenic, the detrimental effects of residual elemental arsenic on the mechanical properties of steel are receiving more and more attention. Nevertheless, arsenic is difficult to remove in the current steelmaking process and thus tends to remain in the final steel products. Due to microsegregation and grain boundary segregation, high concentrations of arsenic weaken grain boundary cohesion and cause the embrittlement of steel.

The temperature from which the liquid alloy is quenched affects the solidification microstructures as well as phase selection, thereby influencing the final mechanical properties. At present, many studies about the effects of element content and solidification cooling method on microstructure and the segregation or precipitation of alloy elements have been performed for Fe-based binary alloys such as Fe–P [2], Fe–Sn [3–4], Fe–Cu [5–6], Fe–Nb [7], Fe–B [8–9], and Fe–Cr [10] alloys; only a few studies have been carried out on Fe–As alloy. Subramanian *et al.* [11] investigated the dendritic segregation characteristics of Fe–10wt%As alloys quenched from various temperatures. Yin [12] found eutectic arsenide in the upper part of the ingot with 6wt%As. The systematic investigation on the solidification microstructure, the segregation of soluble arsenic in the grain boundary, and the characteristics of arsenic-rich phases in Fe–As binary alloys will be greatly beneficial in understanding the mechanism of action of arsenic in steel. It is also essential to thoroughly study the microstructure and distribution of arsenic in Fe–As alloys in order to control the harmfulness of arsenic in steel. However, the effects of arsenic content and quenching temperature on the solidification microstructure and distribution of arsenic in Fe–As alloys have not been determined.

In the present paper, the solidification microstructures of Fe–As binary alloys with different arsenic contents and

Corresponding author: Bo Song E-mail: songbo@metall.ustb.edu.cn

quenching temperatures are systematically studied. Furthermore, microsegregation and grain boundary segregation of soluble arsenic in Fe–As alloys with low arsenic contents are investigated along with the compositions, morphologies, and amounts of arsenic-rich phases in Fe–As alloys with high arsenic contents.

2. Experimental

Fe–As alloys were prepared from pure iron and high purity arsenic (99.9999wt% As) using a high-temperature molybdenum resistance furnace and an FP93 series automatic temperature controller with an accuracy of ± 2°C. About 300 g of pure iron was melted at 1600°C under a purified argon atmosphere in an Al_2O_3 crucible with a diameter of 40 mm and a depth of 100 mm. After stabilization of the melts at 1600°C for 5 min, high purity arsenic was added to produce melts with different arsenic contents. After holding for 10 min, the melts were cooled to different temperatures in the furnace by turning off the power. After quenching with water, ingots of 35 mm in diameter and 42 mm in height were obtained. Table 1 shows the main chemical compositions and cooling methods of the prepared alloys. The Fe–As alloys with different arsenic contents and quenching temperatures in this study are labeled with solid circles in the Fe–As binary phase diagram (Fig. 1).

Table 1. Chemical compositions and cooling methods of the Fe–As alloys

As content / wt%				Cooling method
Fe–0.5%As	Fe–1.5%As	Fe–4%As	Fe–10%As	
0.51	1.50	3.88	9.52	Water-quenching from 1600°C to room temperature
0.51	1.50	3.88	9.53	Furnace-cooling from 1600°C to 1420°C, then holding for 10 min followed by water-quenching
0.50	1.51	3.75	9.18	Furnace-cooling from 1600°C to 1200°C, then holding for 10 min followed by water-quenching
0.52	1.49	3.76	9.20	Furnace-cooling from 1600°C to 850°C, then holding for 10 min followed by water-quenching

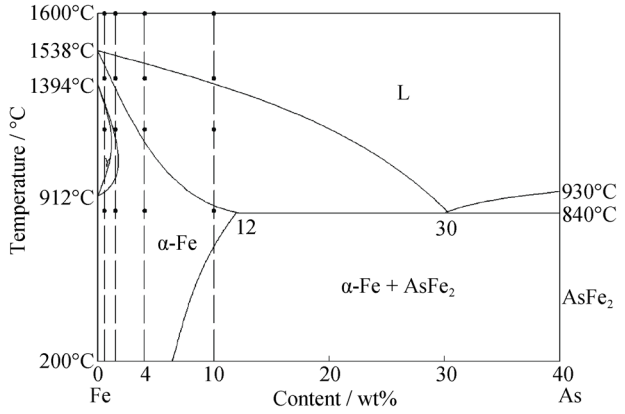

Fig. 1. Fe–As binary partial phase diagram [13].

After the experiments, the samples were cut at a distance of 13 mm away from the bottom of the ingots. The samples were then mechanically ground, polished, and etched with 4vol%–10vol% Nital for metallographic and scanning electron microscopy (SEM) observation. The distributions of arsenic in the Fe–As alloys with low arsenic contents were determined by electron probe microanalysis (EPMA; JXA-8230) and transmission electron microscopy (TEM; JOM 2011). The EPMA analysis was performed on an area of 0.49 mm × 0.49 mm (350 points × 350 points). For TEM examination, 0.4 mm-thick slices were first cut from the samples using a spark line cutting method. They were then manually pre-thinned to 30 μm using waterproof SiC paper. Finally, 3-mm discs were thinned in a twin jet electropolisher using a solution of 5vol% perchloric acid and 95vol% ethanol at −25°C at a voltage of 30 V. For the analysis of grain boundary chemistry, the electron beam spot was adjusted to a diameter of about 1.5 nm, and several grain boundaries for each sample were analyzed to ensure accurate results.

The compositions, morphologies, and area fractions of arsenic-rich phases in samples with high arsenic contents were investigated using SEM with energy dispersive spectroscopy (EDS) and X-ray diffraction (XRD). Ten back-scattered electron (BSE) images were randomly selected for each sample etched by 10vol% Nital. The area fraction of the arsenic-rich phase was taken as the average value of 10 images. XRD was carried out on a TTR III multi-function X-ray diffractometer with Cu K_α radiation at 40 kV and 300 mA. The samples were scanned in the 2θ range of 30°–120° with a scanning speed of $10°\cdot min^{-1}$ and a step space of 0.02°.

3. Results and discussion

3.1. Solidification microstructures of Fe–As alloys

The solidification microstructures of Fe–As alloys are

significantly influenced by the arsenic content. Fig. 2 shows the microstructural changes of Fe–As alloys with increasing arsenic content. The microstructure of the Fe–As alloys quenched from 1420°C changes from irregular ferrite to fully-developed α-Fe dendrites as the arsenic content increases from 0.5wt% to 10wt%. Massive primary α-Fe dendrites and secondary dendrite arms can be clearly observed, especially when the content of arsenic is 4wt%.

The microstructures of Fe–0.5wt%As alloys are not affected by quenching temperature, as shown in Fig. 3. The

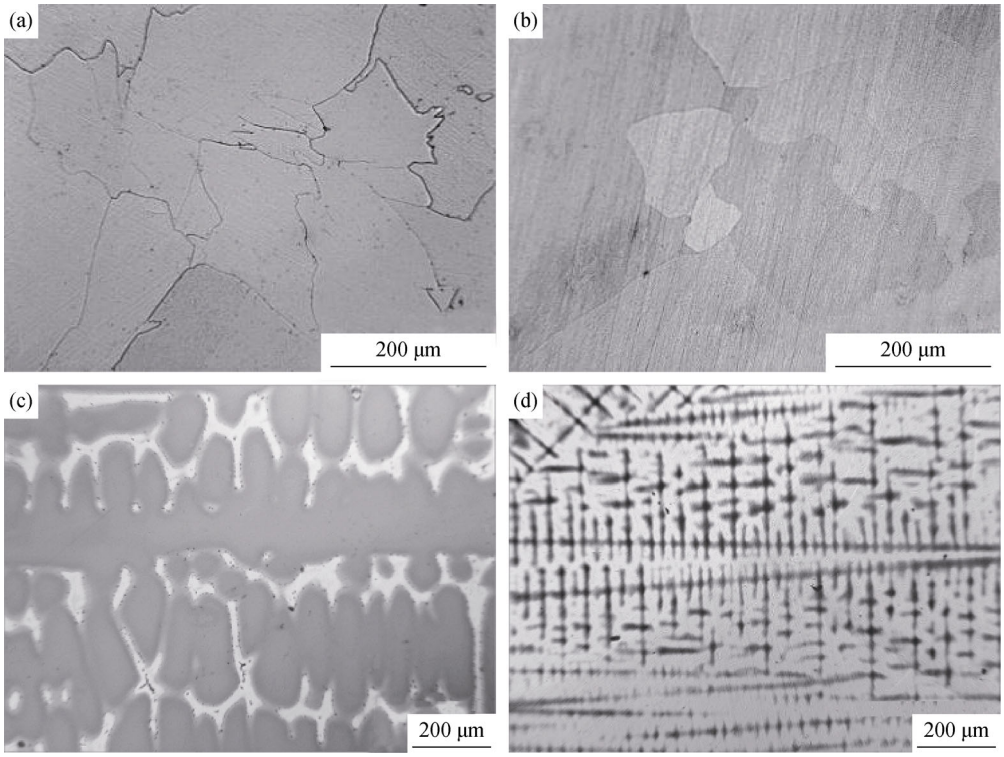

Fig. 2. Microstructures of Fe–As alloys quenched from 1420°C: (a) Fe–0.5wt%As; (b) Fe–1.5wt%As; (c) Fe–4wt%As; (d) Fe–10wt%As.

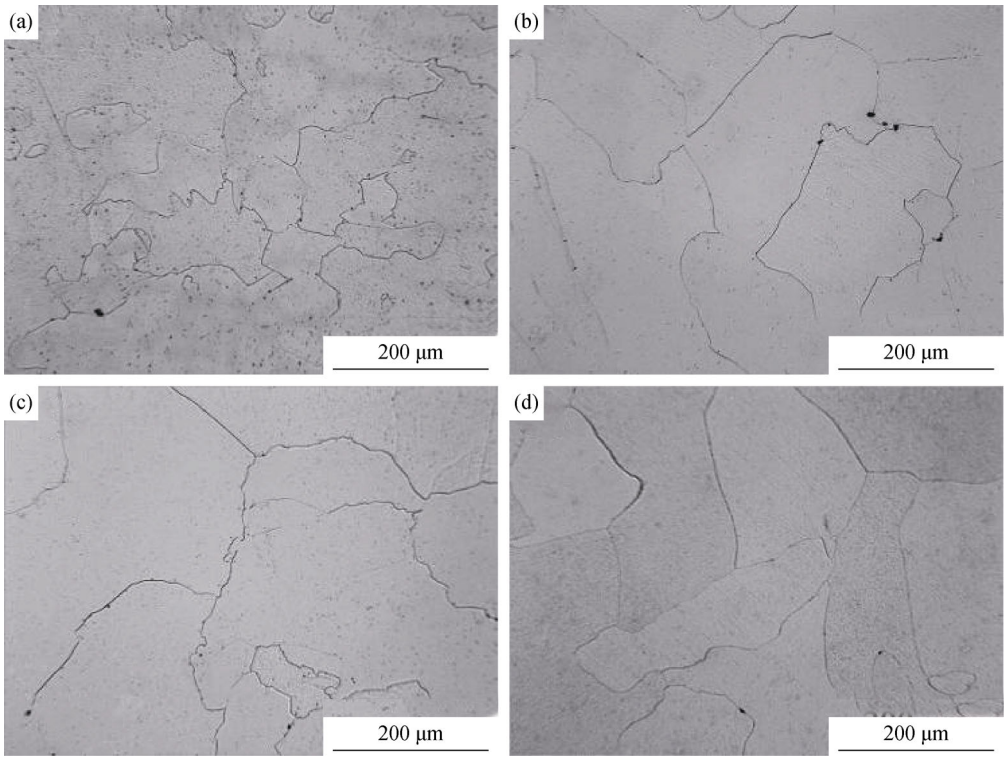

Fig. 3. Microstructures of Fe–0.5wt%As alloys quenched from different temperatures: (a) 1600°C; (b) 1420°C; (c) 1200°C; (d) 850°C.

microstructures of Fe–0.5wt%As alloys are all ferrite with grain sizes ranging from 100 to 300 μm. According to the Fe–As binary phase diagram (Fig. 1), the liquidus temperature of Fe–0.5wt%As alloys is about 1530°C, and this alloy displays a narrow freezing range. Thus, Fe–0.5wt%As alloys quenched from 1420, 1200, and 850°C are all located in the solid phase region before quenching. This explains why the solidification microstructures shown in Figs. 3(b)–3(d) are quite similar.

The microstructural variation among the Fe–4wt%As and Fe–10wt%As alloys with different quenching temperatures is shown in Fig. 4. It should be noted that the microstructures of Fe–4wt%As and Fe–10wt%As alloys with the lower quenching temperatures are not given because their microstructures are difficult to be etched out using 10vol% Nital. It can be seen from Fig. 4 that a clear dendritic morphology is observed in the alloys. Furthermore, the white network structure is clearly observed in the Fe–10wt%As alloy quenched from 1200°C (Fig. 4(e)). Therefore, it can be concluded that the microstructures of Fe–As alloys with high arsenic contents are composed of α-Fe dendrites and interdendritic compounds. Detailed information about the composition, morphology, and distribution of the interdendritic compounds in these alloys will be subsequently revealed by SEM observations. Fig. 5 shows the effects of arsenic content and quenching temperature on secondary dendrite arm spacing in Fe–4wt%As and Fe–10wt%As alloys, which were measured by the mean linear intercept method. It is evident that a higher quenching temperature results in finer α-Fe dendrites for the same concentration of arsenic. For Fe–4wt%As alloys, quenching from 1600°C is a rapid solidification process, whereas quenching from 1420°C includes 10 min of holding in the liquid-solid two-phase region before cooling; thus, the α-Fe dendrites are large

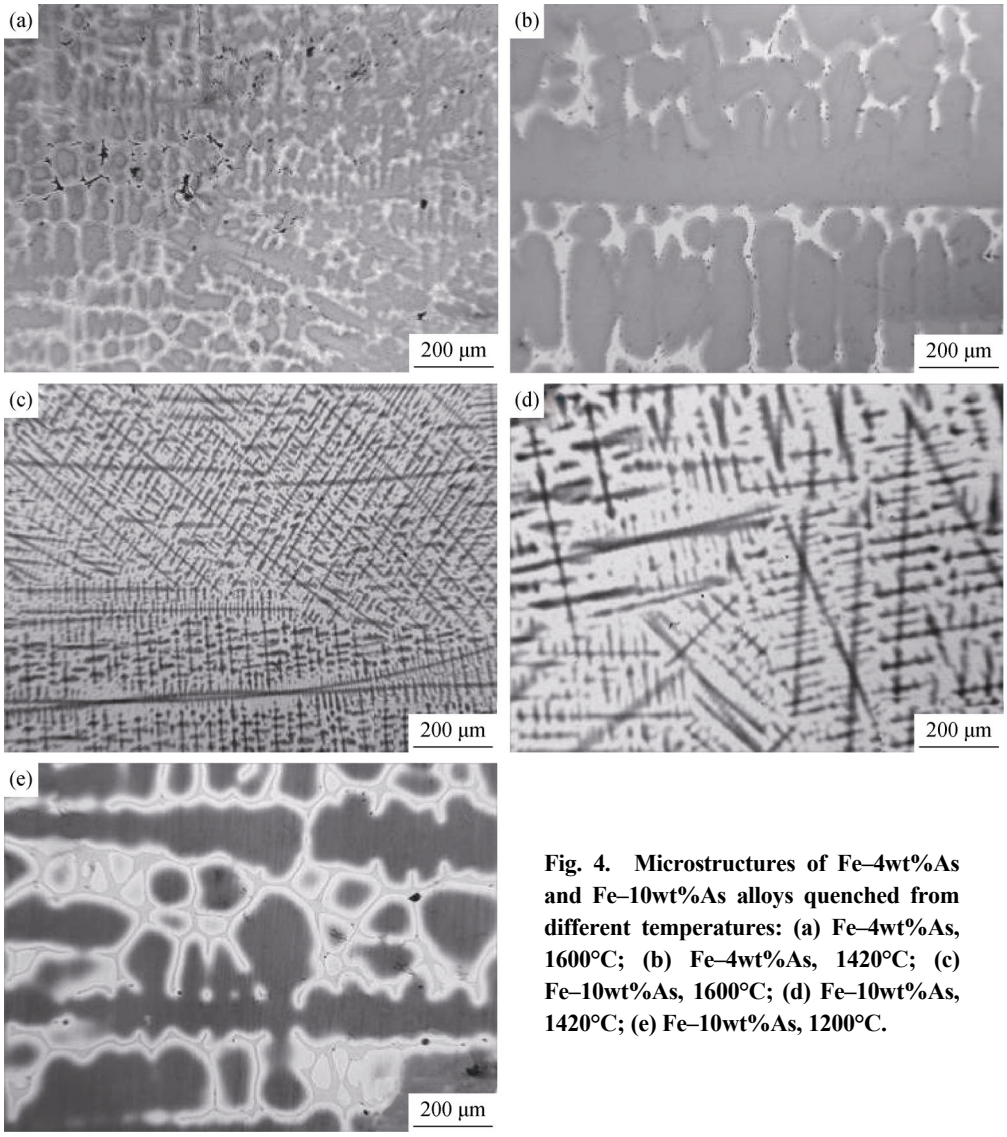

Fig. 4. Microstructures of Fe–4wt%As and Fe–10wt%As alloys quenched from different temperatures: (a) Fe–4wt%As, 1600°C; (b) Fe–4wt%As, 1420°C; (c) Fe–10wt%As, 1600°C; (d) Fe–10wt%As, 1420°C; (e) Fe–10wt%As, 1200°C.

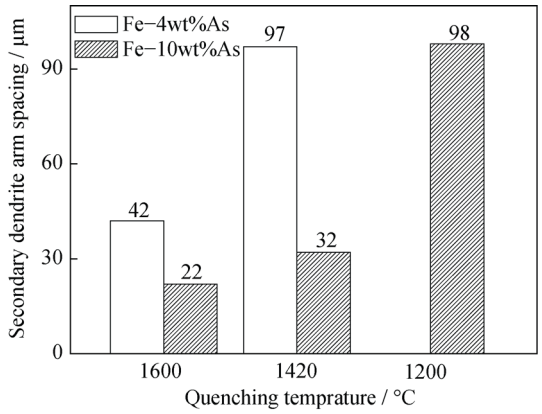

Fig. 5. Relationship between secondary dendrite arm spacing and quenching temperature in Fe–4wt%As and Fe–10wt%As alloys.

because they are allowed to grow for 10 min. For Fe–10wt%As alloys quenched from 1600 and 1420°C, the α-Fe dendrites in the former case are finer than those in the latter case, even though both temperatures lie in the liquid phase region. This occurs because the higher quenching temperature results in a shorter time for solidification and growth [14]. In addition, the α-Fe dendrites become finer with increasing arsenic content from 4wt% to 10wt% at the same quenching temperature. The finer α-Fe dendrites may result from an increase in the α-Fe nucleation probability in liquid with increasing arsenic content. A similar phenomenon was observed in Re-containing cast Ni-base superalloys with different Cr contents [15].

3.2. Distribution of arsenic

3.2.1. Microsegregation and grain boundary segregation of arsenic in the case of low arsenic content

Fig. 6 shows the distribution of soluble arsenic in Fe–0.5wt%As alloys quenched from 1600 and 1200°C. For both of the alloys, arsenic solidification microsegregation was not observed by EPMA. This result is consistent with

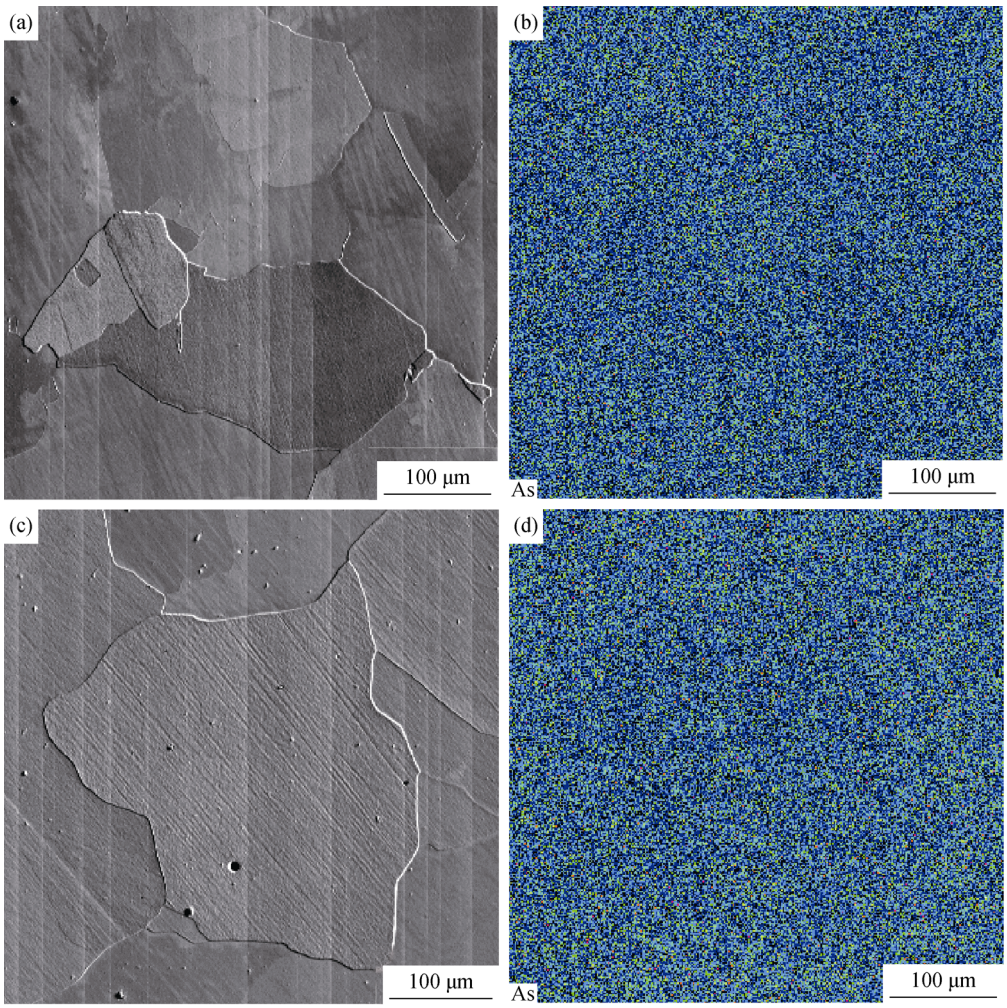

Fig. 6. Distribution of soluble arsenic revealed by EPMA in Fe–0.5wt%As alloys quenched from 1600 and 1200°C: (a) EPMA microstructure image, 1600°C; (b) mapping result of arsenic, 1600°C; (c) EPMA microstructure image, 1200°C; (d) mapping result of arsenic, 1200°C.

the autoradiography findings of Oi and Sato [16], who have not detected arsenic microsegregation in the grain interior in the cast Fe–0.21wt%^{76}As alloy. Generally, very high cooling rate will suppress or eliminate element microsegregation due to the lack of time for element redistribution during steel solidification. Therefore, it is reasonable that arsenic microsegregation is not found in Fe–0.5wt%As quenched from 1600 and 1200°C. Although there is no arsenic microsegregation, soluble arsenic tends to segregate at grain boundaries [17–18]. Fig. 7 shows the TEM micrographs of grain boundaries in Fe–0.5wt%As alloys quenched from 1600 and 1200°C. EDS results in Table 2 show that the average arsenic concentration at the grain boundaries is almost 1.5-times higher than that in the matrix, regardless of quenching temperature. Consequently, in the case of low arsenic content, the microsegregation of soluble arsenic does not appear only except near the grain boundaries.

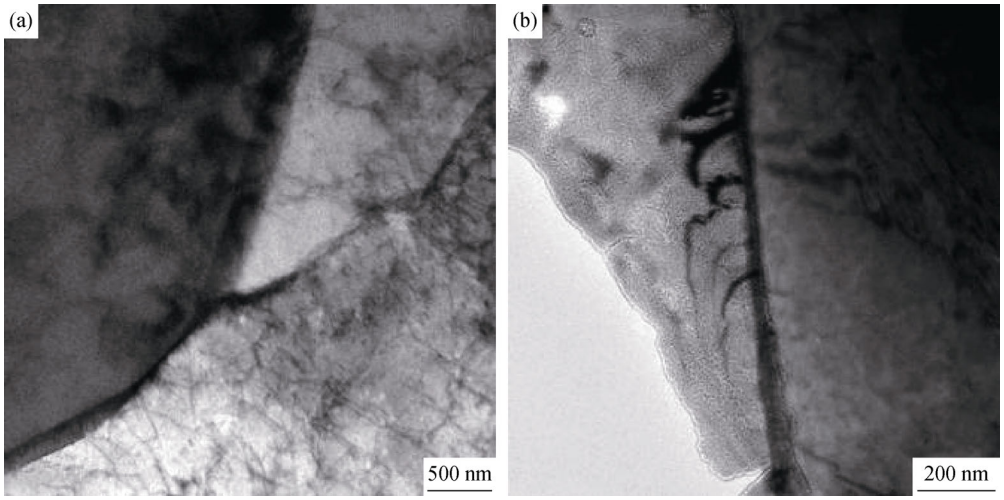

Fig. 7. Typical grain boundary micrographs of Fe–0.5wt%As alloys quenched from 1600°C (a) and 1200°C (b).

Table 2. EDS results for the grain boundaries (GB) and matrix of Fe–0.5wt%As alloys quenched from 1600 and 1200°C wt%

Temperature / °C	Position	1	2	3	4	5	Average
1600	GB	0.57	0.68	0.54	0.66	0.52	0.59
	Matrix	0.40	0.56	0.36	0.58	0.16	0.41
1200	GB	0.66	0.83	0.51	0.35		0.59
	Matrix	0.51	0.64	0.29	0.26		0.42

3.2.2. Composition, morphology, and distribution of arsenic-rich phases in the case of high-arsenic content

The eutectic morphology and the composition of eutectic phases in hypoeutectic alloys might change depending on the composition and the cooling method [19–21]. As shown in Fig. 8, Fe–4wt%As and Fe–10wt%As alloys quenched from 1420°C have the same eutectic morphology, which is obviously different from that of the Fe–10wt%As alloy quenched from 1200°C. Although the eutectic morphology is different, the EDS-determined composition of the white interdendritic eutectic phase in these three alloys is similar. Furthermore, α-Fe and Fe_2As phases are detected by XRD in Fe–10wt%As alloys quenched from 1420 and 1200°C (Fig. 9). It can be concluded from the EDS and XRD results that the white interdendritic eutectic phase in the studied alloys is Fe_2As.

SEM images in Fig. 10 show the eutectic morphologies in Fe–4wt%As and Fe–10wt%As alloys with different quenching temperatures. The distribution, morphology, and amount of the eutectic phase are greatly influenced by arsenic content and quenching temperature. The white eutectic Fe_2As phase distributes discontinuously in the interdendritic regions of Fe–4wt%As and Fe–10wt%As alloys quenched from 1600 and 1420°C, whereas the eutectic Fe_2As phase forms a continuous network structure in Fe–10wt%As alloy quenched from 1200°C. For Fe–4wt%As and Fe–10wt%As alloys quenched from 1600 and 1420°C, the eutectic morphologies shown in Figs. 10(a)–10(e) are fully divorced. When the quenching temperature decreases to 1200°C in Fe–10wt%As alloys, the eutectic microstructure changes to fibrous and is composed of the white interdendritic eutectic Fe_2As phase and the interior rod-like eutectic α-Fe phase

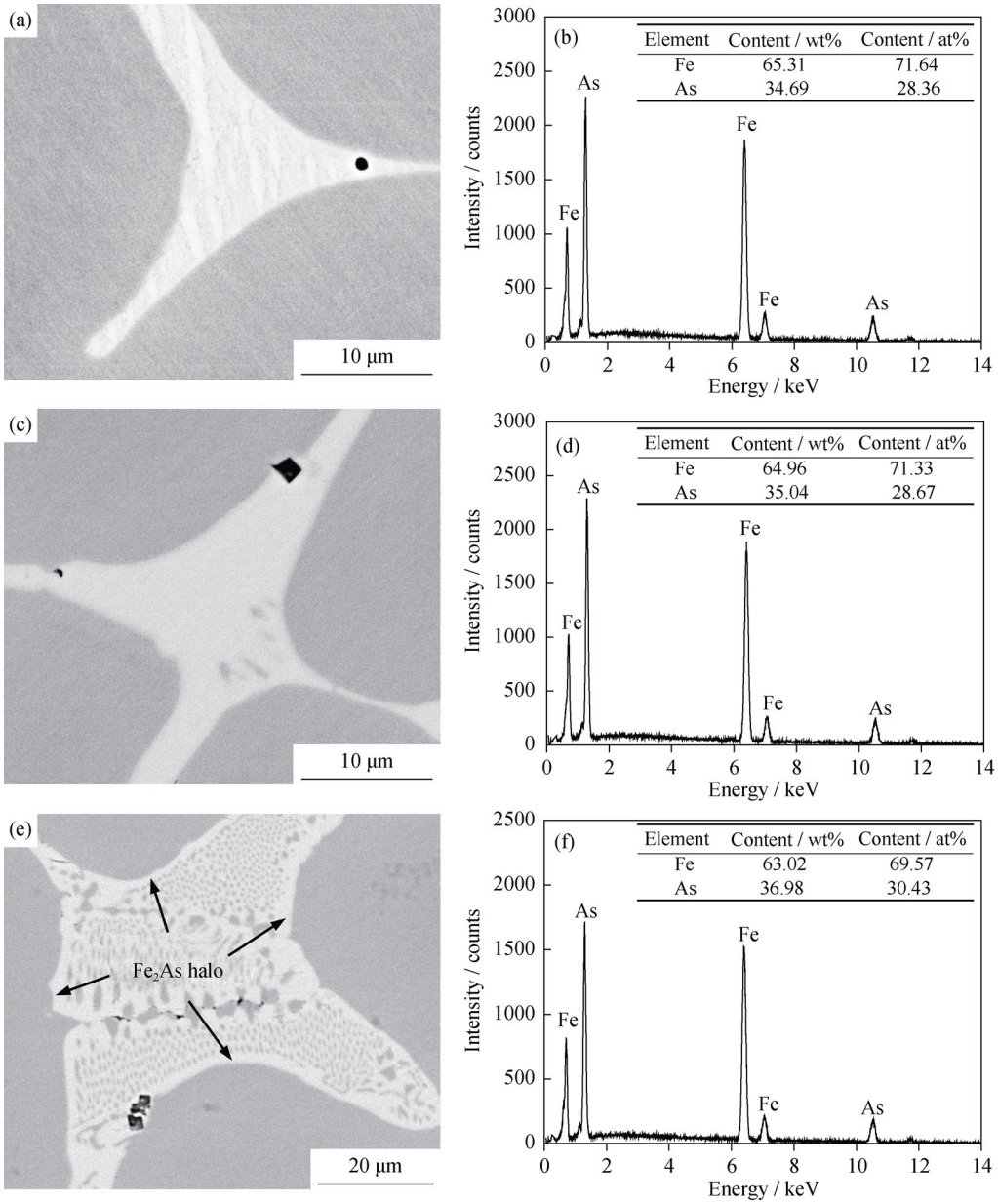

Fig. 8. BSE micrographs and EDS spectra of arsenic-rich phases in Fe–4wt%As and Fe–10wt%As alloys: (a, b) Fe–4wt%As, 1420°C; (c, d) Fe–10wt%As, 1420°C; (e, f) Fe–10wt%As, 1200°C.

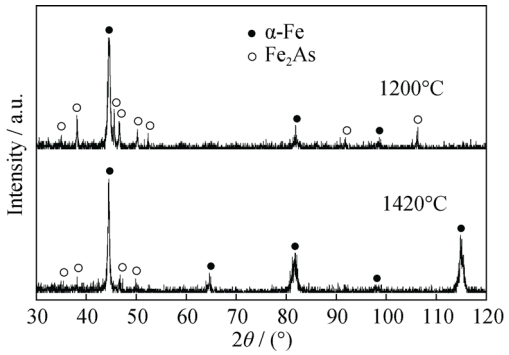

Fig. 9. XRD patterns of Fe–10wt%As alloys quenched from 1200 and 1420°C.

(Figs. 8(e) and 10(f)). In addition, Fig. 8(e) shows that the eutectic α-Fe and primary α-Fe dendrites are isolated by a white Fe_2As halo, and that the eutectic Fe_2As phase is connected with the white halo. This indicates that the eutectic Fe_2As phase acts as a preliminary phase during the eutectic reaction process. Fig. 11 shows the effects of arsenic content and quenching temperature on the area fraction of the eutectic Fe_2As phase. The results indicate that the amount of eutectic Fe_2As phase increases with increasing arsenic content from 4wt% to 10wt% and decreasing quenching temperature from 1600 to 1200°C.

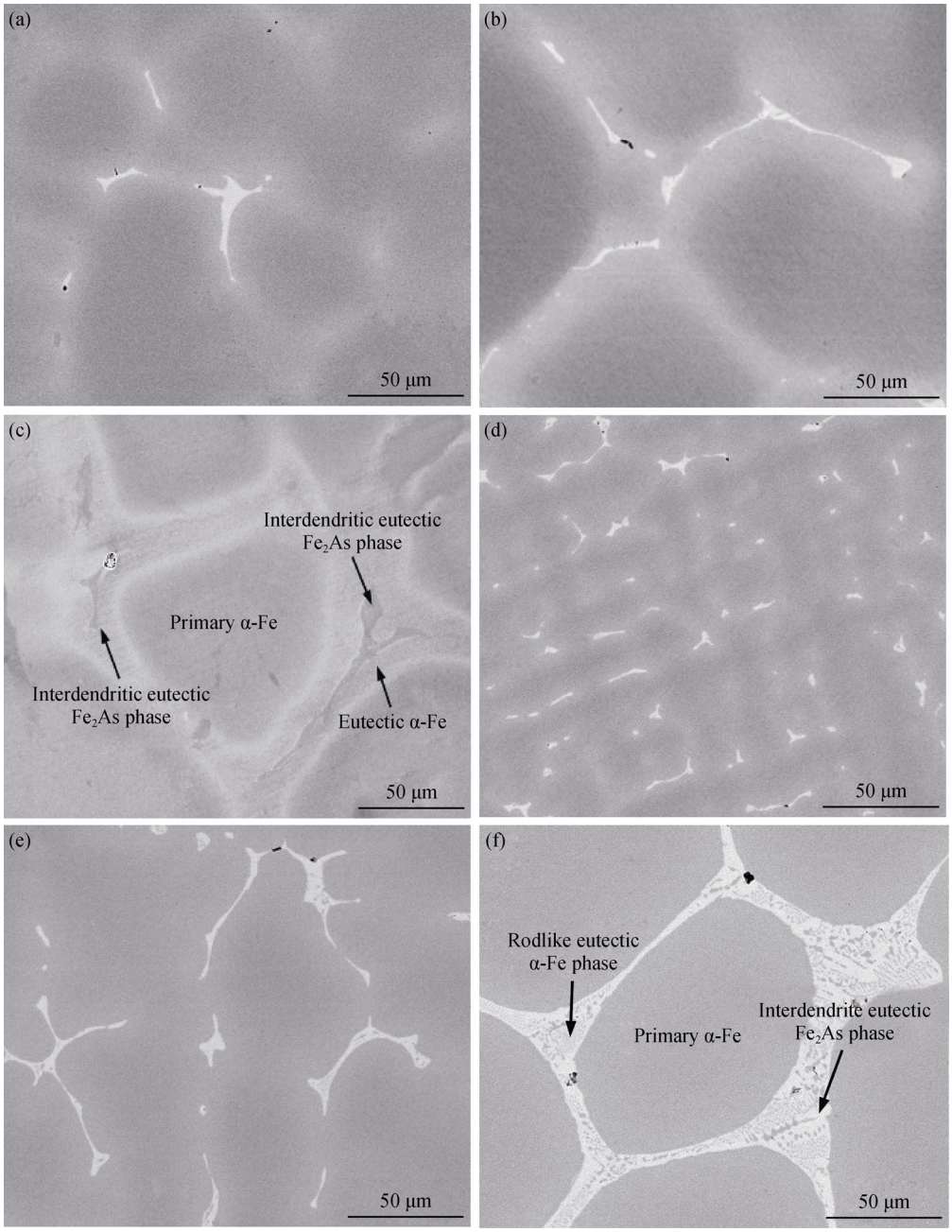

Fig. 10. SEM images showing the eutectic microstructures in Fe–4wt%As and Fe–10wt%As alloys: (a) Fe–4wt%As, 1600°C, BSE; (b) Fe–4wt%As, 1420°C, BSE; (c) Fe–4wt%As, 1420°C, secondary electron image; (d) Fe–10wt%As, 1600°C, BSE; (e) Fe–10wt%As, 1420°C, BSE; and (f) Fe–10wt%As, 1200°C, BSE.

According to the Fe–As binary phase diagram [13], there is no eutectic microstructure in the Fe–4wt%As and Fe–10wt%As alloys during the equilibrium solidification process. However, a metastable eutectic microstructure can be formed during the non-equilibrium solidification process. As non-equilibrium solidification proceeds, the primary α-Fe dendrites preferentially nucleate and grow, and arsenic is thus gradually enriched in the interdendritic regions. When the temperature and arsenic concentration of the residual liquid reach 840°C and 30wt%, respectively, the eutectic reaction (L → α-Fe + Fe_2As) occurs. The formation of fully divorced and fibrous eutectic morphologies mainly depends on the volume fraction of the interdendritic liquid. For low volume fractions of interdendritic liquid, the eutectic α-Fe phase preferentially grows and attaches to the primary α-Fe phase during the eutectic reaction process; as a result, the eutectic Fe_2As phase is formed only in the last solidification interdendritic liquid, and a fully-divorced eutec-

tic morphology is observed in Figs. 10(a)–10(e). For high volume fractions of interdendritic liquid, the eutectic Fe_2As phase is the preliminary phase, as demonstrated by the Fe_2As halo seen in Fig. 8(e). Its growth inevitably consumes large amounts of As atoms from the adjacent liquid, accelerating the nucleation of the eutectic α-Fe phase. The fibrous morphology observed in Figs. 8(e) and 10(f) is formed by the alternative nucleation and growth of eutectic Fe_2As and α-Fe phases. Higher quenching temperature will produce finer primary α-Fe dendrites, confining the eutectic solidification into the smaller interdendritic regions. This results in a lower volume fraction of interdendritic liquid. Higher quenching temperature also increases the average undercooling required for the nucleation of the eutectic phase. Therefore, the eutectic microstructure is frequently more divorced at higher quenching temperatures [22].

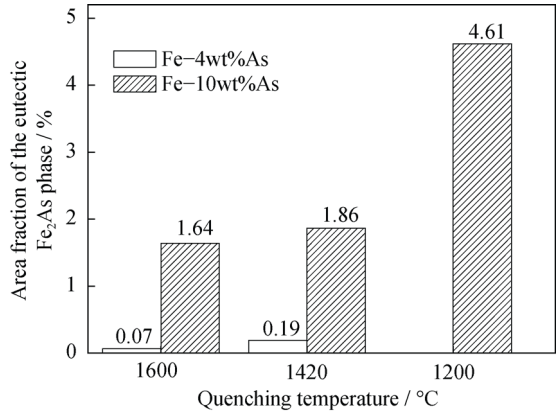

Fig. 11. Area fraction of the eutectic Fe_2As phase in Fe–4wt%As and Fe–10wt%As alloys.

4. Conclusions

(1) As the arsenic content increases from 0.5wt% to 10wt%, the microstructure of Fe–As alloys quenched from 1420°C changes from irregular ferrite to typical α-Fe dendrites. The microstructures of Fe–0.5wt%As alloys quenched from different temperatures are all irregular ferrite, while the microstructures of Fe–4wt%As and Fe–10wt%As alloys quenched from different temperatures are typical α-Fe dendrites. The α-Fe dendrites become finer with increasing quenching temperature from 1200 to 1600°C and increasing arsenic content from 4wt% to 10wt%.

(2) Solidification microsegregation of arsenic is not observed by EPMA in Fe–0.5wt%As alloys quenched from 1600 and 1200°C. However, the average arsenic concentration at the grain boundaries in the two alloys detected by TEM is higher than that in the matrix.

(3) For Fe–4wt%As and Fe–10wt%As alloys quenched from 1600 and 1420°C, the eutectic morphology is fully divorced, and the white eutectic Fe_2As phase distributes discontinuously in the interdendritic regions. In contrast, the eutectic morphology of Fe–10wt%As alloy quenched from 1200°C is fibrous and forms a continuous network structure. Moreover, increasing arsenic content and decreasing quenching temperature increase the area fraction of the eutectic Fe_2As phase.

Acknowledgements

This work was financially supported by the National Natural Science Foundation of China (No. 51174019).

References

[1] A.P. Xian, D. Zhang, and Y.K. Wang, Impurities in steel and their influence on steel properties, *Iron steel*, 34(1999), No. 10, p. 64.

[2] M. Suzuki, T.J. Piccone, M.C. Flemings, and H.D. Brody, Solidification of highly undercooled Fe–P alloys, *Metall. Trans. A*, 22(1991), No. 11, p. 2761.

[3] B. Predel and M. Frebel, Precipitation behavior of α-solid solutions of the Fe–Sn system, *Metall. Trans.*, 4(1973), No. 1, p. 243.

[4] Z.Z. Liu, M. Kuwabara, R. Satake, and T. Nagata, Effect of Sn on microstructure and sulfide precipitation in ultra low carbon steel, *ISIJ Int.*, 49(2009), No. 7, p. 1087.

[5] Y. Yuan, K. Sassa, K. Iwai, Q. Wang, J.C. He, and S. Asai, Copper distribution in Fe–Cu and Fe–C–Cu alloys under imposition of an intense magnetic field, *ISIJ Int.*, 48(2008), No. 7, p. 901.

[6] Z. Chen, F. Liu, H.F. Wang, W. Yang, G.C. Yang, and Y.H. Zhou, Formation of single-phase supersaturated solid solution upon solidification of highly undercooled Fe–Cu immiscible system, *J. Cryst. Growth*, 310(2008), No. 24, p. 5385.

[7] M. Kudoh, M. Tezuka, and K. Matsuura, Effect of niobium on the formation of microstructure and grain boundary in Fe–Nb and Fe–C–Nb alloys, *ISIJ Int.*, 46(2006), No. 12, p. 1871.

[8] D.W. Yi, J.D. Xing, S.Q. Ma, H.G. Fu, Y.F. Li, W. Chen, J.B. Yan, J.J Zhang, and R.R. Zhang, Investigations on microstructures and two-body abrasive wear behavior of Fe–B cast alloy, *Tribol. Lett.*, 45(2012), No. 3, p. 427.

[9] S.Q. Ma, J.D. Xing, G.F. Liu, D.W. Yi, H.G. Fu, J.J. Zhang, and Y.F. Li, Effect of chromium concentration on microstructure and properties of Fe–3.5B alloy, *Mater. Sci. Eng. A*, 527(2010), No. 26, p. 6800.

[10] X.Z. Zhang, Solidification modes and microstructure of Fe–Cr alloys solidified at different undercoolings, *Mater. Sci. Eng. A*, 247(1998), No. 1-2, p. 214.

[11] S.V. Subramanian, C.W. Haworth, and D.H. Kirkwood, Development of interdendritic segregation in an iron-arsenic al-

loy, *J. Iron Steel Inst.*, 206(1968), No. 11, p. 1124.

[12] G.J. Yin, The distribution of arsenic in steel, *Iron steel*, 16(1981), No. 2, p. 20.

[13] H. Okamoto, The As–Fe (arsenic–iron) system, *J. Phase Equilib.*, 12(1991), No. 4, p. 457.

[14] L. Zhou, N. Wang, L. Zhang, and W.J. Yao, The effects of the minority phase on phase separation in Fe–Sn hypermonotectic alloy, *J. Alloys Compd.*, 555(2013), p. 88.

[15] X.R. Guan, E.Z. Liu, Z. Zheng, Y.S. Yu, J. Tong, and Y.C. Zhai, Solidification behavior and segregation of Re-containing cast Ni-base superalloy with different Cr content, *J. Mater. Sci. Technol.,* 27(2011), No. 2, p. 113.

[16] T. Oi and K. Sato, Autoradiography of Fe–As and Fe–Sn dilute alloys II: grain boundary segregation of the alloying elements, *Trans. Jpn. Inst. Met.*, 10(1969), No. 1, p. 39.

[17] Y.Z. Zhu, J.C. Li, D.M. Liang, and P. Liu, Distribution of arsenic on micro-interfaces in a kind of Cr, Nb and Ti microalloyed low carbon steel produced by a compact strip production process, *Mater. Chem. Phys.*, 130(2011), No. 1-2, p. 524.

[18] Y.Z. Zhu, Z. Zhu, and J.P. Xu, Grain boundary segregation of minor arsenic and nitrogen at elevated temperatures in a microalloyed steel, *Int. J. Miner. Metall. Mater.*, 19(2012), No. 5, p. 399.

[19] M.S. Dargusch, M. Nave, S.D. McDonald, and D.H. StJohn, The effect of aluminium content on the eutectic morphology of high pressure die cast magnesium–aluminium alloys, *J. Alloys Compd.*, 492(2010), No. 1-2, p. L64.

[20] T.P. Zhu, Z.W. Chen, and W. Gao, Effect of cooling conditions during casting on fraction of β-$Mg_{17}Al_{12}$ in Mg–9Al–1Zn cast alloy, *J. Alloys Compd.*, 501(2010), No. 2, p. 291.

[21] C. Fan, S.Y. Long, H.D. Yang, X.J. Wang, and J.C. Zhang, Influence of Ce and Mn addition on α-Fe morphology in recycled Al–Si alloy ingots, *Int. J. Miner. Metall. Mater.*, 20(2013), No. 9, p. 890.

[22] D.H. St John, A.K. Dahle, T. Abbott, M.D. Nave, and M. Qian, Solidification of cast magnesium alloys, [in] *The* 2003 *TMS Annual Meeting*, San Diego, 2003, p. 95.